EOS
EOS, TRANSACTIONS, AMERICAN GEOPHYSICAL UNION

VOLUME 88 NUMBER 9
27 FEBRUARY 2007
PAGES 105–116

Risk of Rising Sea Level to Population and Land Area

PAGES 105, 107

Low-elevation land areas and their populations are at risk globally from rising sea level. Global sea level has risen by about 2 millimeters per year over the past century. About half of this rise may be attributed to thermal expansion of the ocean and the melting of temperate-latitude glaciers [*Dyurgerov and Meier*, 1997]. The remainder of the rise is believed to come from a net loss of mass from the Antarctic and Greenland ice sheets, although the exact contribution is unknown.

Throughout the next century, the rate of sea level rise is expected to increase due to greenhouse warming, with the Fourth Assessment Report of the Intergovernmental Panel on Climate Change (IPCC) concluding that the rise of global average sea level by 2100 will be in the range from 18–38 to 26–59 centimeters depending on the emissions scenario [*IPCC*, 2007]. However, this assessment does not take into account the rapid changes in ice sheet mass flux that have been observed since 2003 [e.g., *Rignot and Kanagaratam*, 2006], and therefore actual sea level changes may be larger than predicted by the IPCC.

If the rate of sea level rise increases substantially, it will cause serious and direct environmental impacts to many low-lying coastal areas around the world. Such impacts include increased beach erosion, loss of vital agricultural and cultural resources, and, as we will show here, potential inundation of thousands of square kilometers of coastal land and the resulting displacement of millions of coastal residents. These outcomes will be complex and in some cases may be mitigated, but it is important to understand their general scope.

Using recently produced global elevation and population data sets, we took an 'inundation' approach to determine land area lost and current population affected by hypothetical sea level increases between 1 and 6 meters.

By R. J. Rowley, J. C. Kostelnick, D. Braaten, X. Li, and J. Meisel

Elevation and Population Data Sets

Inundation zones were calculated from the Global Land One-Kilometer Base Elevation (GLOBE) digital elevation model (DEM) [*Hastings and Dunbar*, 1998], a raster (i.e., gridded) elevation data set covering the entire world. Cells in GLOBE have a spatial resolution of 30 arc seconds of latitude and longitude (approximately 1 kilometer at the equator), with each land cell in the grid assigned an elevation value (meters) in whole-number increments. GLOBE was developed through a collaboration of international experts and was compiled from the best global and regional raster (e.g., DEMs) and vector (e.g., contours) elevation data sets available at the time of compilation.

In addition to GLOBE, inundation zones were also computed from the ETOPO2 raster elevation data set developed by the NOAA National Geophysical Data Center (NGDC) [*NOAA NGDC*, 2001]. The coarser resolution of ETOPO2 (2 minutes of latitude and longitude; approximately 3.7 kilometers at the equator) is ideal for visualizing the inundation process on a map animation of the entire world (see available products, discussed below).

Populations in the inundation zones were estimated from LandScan, a global population data set developed by the Oak Ridge National Laboratory Global Population Project for estimating populations at risk [*Dobson et al.*, 2000]. LandScan was compiled from the best available population census data for each country that were then disaggregated into cells based on land cover type, proximity to roads, slope, and nighttime lights (see *Dobson et al.* [2000] for discussion of the data sets and methods used to develop LandScan as well as data set validation and verification results). LandScan has been used for a variety of humanitarian applications, such as estimating populations affected by natural disasters and wartime conflicts. A particular advantage of using LandScan in this study is that the spatial res-

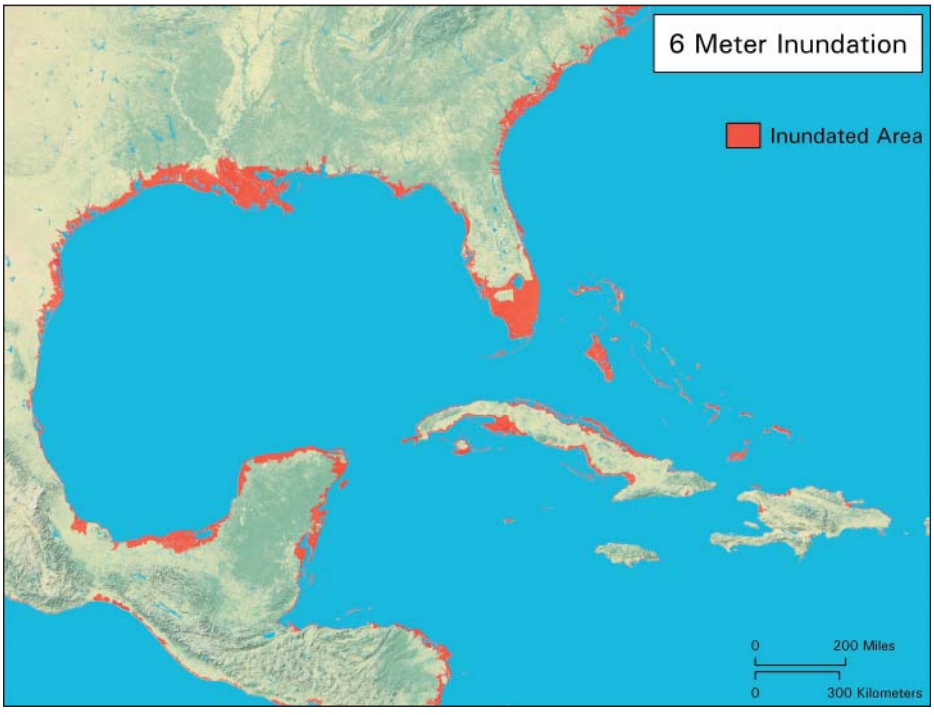

Fig. 1. Inundation of 6 meters (in red) for portions of the southeastern United States, Central America, and the Caribbean. Land cover and shaded relief map from Natural Earth, Tom Patterson, U.S. National Park Service.

Table 1. Total Surface Area Inundated and Population at Risk at Global and Regional Scales[a]

Sea Level Rise, m	Inundated Area, × 1000 km^2	Population Affected, millions
Global Results[b]		
1	1054.99	107.94
2	1312.97	175.10
3	1538.58	233.99
4	1775.24	308.08
5	2004.37	376.26
6	2193.30	431.44
Sea Level Rise, m	Inundated Area, × 1000 km^2	Population Affected
Regional Results		
Southeast Asia and northern Australia (A)		
1	347.68	46,683,288
2	426.24	86,138,352
3	483.29	114,024,464
4	537.56	153,082,944
5	588.47	183,449,216
6	630.49	209,142,000
Southeastern United States (B)		
1	62.28	2,639,650
2	104.51	5,492,852
3	137.35	8,706,661
4	164.76	13,217,481
5	190.62	17,086,124
6	210.40	19,271,168
The Mediterranean (C)		
1	18.69	4,779,785
2	25.76	6,911,510
3	33.31	9,296,516
4	39.67	11,372,060
5	49.28	14,748,948
6	57.68	18,310,940
Northwestern Europe (D)		
1	34.70	12,242,182
2	41.97	14,500,142
3	49.78	17,136,026
4	55.54	18,915,032
5	64.62	21,717,756
6	69.20	23,069,594
Alaska (E)		
1	47.83	25,981
2	53.43	29,803
3	61.42	34,678
4	67.75	38,879
5	75.65	47,069
6	82.20	50,580
Amazon Delta Region (F)		
1	163.55	13,557,709
2	189.67	15,704,764
3	207.38	17,876,700
4	225.65	19,683,310
5	240.49	21,595,304
6	255.21	23,085,576
East Asia (G)		
1	15.25	11,198,407
2	26.13	25,107,112
3	45.26	41,883,924
4	63.68	58,662,000
5	88.50	78,512,872
6	103.26	94,926,888
South Asia (H)		
1	26.67	10,633,752
2	43.38	24,862,416
3	63.10	40,199,420
4	103.94	71,463,576
5	125.33	89,797,168
6	143.29	103,521,560

[a]Note that in areas of overlap in regions (see Figure 2), the population and land area inundated within that overlap obviously are included in more than one regional total.
[b]As reported by X. Li et al. (submitted manuscript, 2006).

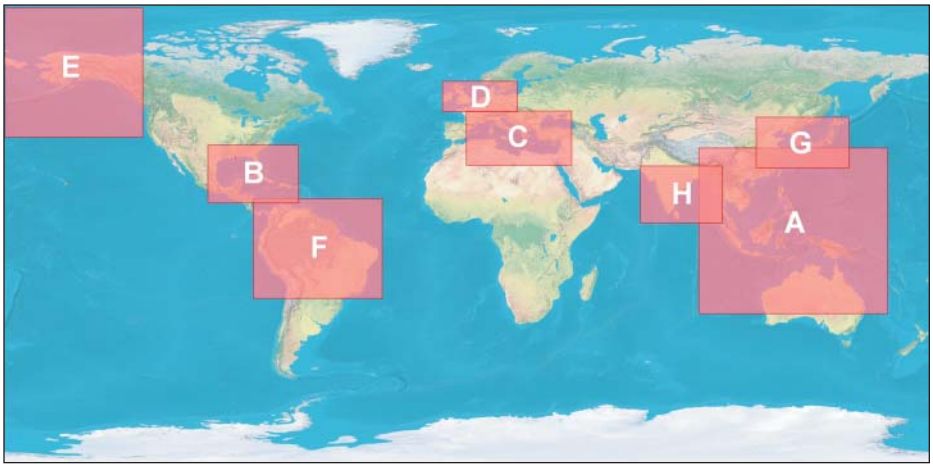

Fig. 2. Regions used for land area and population calculations in Table 1. Land cover and shaded relief map from Natural Earth, Tom Patterson, U.S. National Park Service.

olution is identical to GLOBE (30 arc seconds), which allows for easy calculation of the estimated population in each inundated cell. A potential disadvantage is that, as with any global population data set, the precision and accuracy of population census data vary by country, and any error resulting from these factors undoubtedly will be propagated through the results of this research. The most recent version of LandScan (2004) was used for all population calculations in the inundation zones.

GIS Methodology

Potentially inundated areas were computed based on elevation and proximity to the current ocean shoreline. To accomplish this, we developed an iterative, two-step custom algorithm in a geographic information systems (GIS) raster analysis framework. First, the algorithm flags all raster cells in the DEM that lie adjacent to the contiguous ocean. Second, cells within that group of flagged cells whose elevation values are less than or equal to the desired sea level rise increment are selected and reassigned as ocean cells. For example, to determine an inundation area for a sea level increase of 1 meter above the current sea level, all cells in the DEM that are adjacent to the ocean and that have a value less than or equal to 1 are selected and converted to water (i.e., they are inundated in the resulting output).

Since the initial pass floods only those cells that are directly adjacent to the current ocean, the two-step procedure is repeated until all cells connected with cells adjacent to the ocean are inundated. A large, flat coastal plain whose elevation is 1 meter above current sea level, for instance, would be inundated after the algorithm has completed several iterations, or until there are no more raster cells of a specific elevation that are adjacent to the current sea level (Figure 1). We completed this process for a rise in sea level at whole-meter increments, from 1 to 6 meters. The output is six raster GIS layers, each showing how the world's shorelines would exist if sea level were to rise for each increment.

Once sea level rise was simulated, we calculated a zone of inundation for each incremental rise. These zones essentially include all flooded cells minus preexisting inland water bodies. Lake Okeechobee, for example, becomes part of the inundated Florida coast, but since it is water already, the cells that represent the lake were removed from the total inundation zone (see Figure 1). By removing these inland water bodies, more accurate inundation areas may be computed for the globe and for regions of particular interest.

Using these modified inundation zones, we estimated area of land inundated and population affected by each sea level rise increment. Employing a raster data set where each cell, at the same resolution as the GLOBE DEM, stores the area for that cell at its particular location on the Earth, we computed the total surface area inundated by simply summing up the area cell values that lie within the inundation zone. This additional data set was necessary for determining the actual surface area since the 30-second × 30-second cells in the GLOBE data set have a different surface area as meridians converge with an increase in latitude. Along with a land area calculation, we also estimated current population in each inundation zone according to the LandScan 2004 data set using a procedure similar to sum cell values in the population data set (i.e., people per cell).

We also produced several maps of inundation at global and regional scales and developed interactive map animations for use in education and public awareness activities for global climate change. The animations make use of our ability to simulate the progression of inundation at steps smaller than whole-meter increments by using several intermediate passes of the two-step algorithm described above.

Effects on Land and People

Table 1 details the results of the land area and the population affected by sea level rise for increments of 1–6 meters. We have included global totals (see X. Li et al., GIS

analysis of global inundation impacts from sea-level rise, submitted to *Transactions in GIS*, 2006, hereinafter referred to as X. Li et al., submitted manuscript, 2006) as well as the totals for several regions of particular interest (Figure 2). These regions are areas of high population density with economic importance and political influence that, as the results indicate, would sustain marked impacts resulting from sea level rise. The impacts are definitely evident when taking into account population alone, yet the large amount of high-value property for residential, agricultural, and industrial uses is another important impact that needs further investigation. Note specifically the map of inundated areas for 6 meters (Figure 1) in the southeastern United States and the corresponding land area and population affected numbers in Table 1. Equally important in this work is the warning of potential humanitarian crises that are likely to occur as a result of coastal inundation in economically less developed regions with high population densities (e.g., South Asia and Southeast Asia). A hint of such crises, and the accompanying socioeconomic impacts, was felt worldwide in the fallout of the Indian Ocean tsunami of 2004.

Determining an inundation zone for anything less than whole-meter increments is impossible because the vertical resolution of the DEMs used here is whole meters. Yet knowing the land area and population that would be affected by submeter rises in sea level could be illuminating as to more near term impacts of sea level rise. This was accomplished through an interpolation procedure as documented by X. Li et al. (submitted manuscript, 2006).

Several products from this research are now available for use by educators, researchers, policy-makers, and other interested individuals. These products include (1) inundation layers that are viewable in the virtual globe Google Earth©; (2) global and regional static maps of sea level rise (in both PDF and JPEG formats); (3) global and regional map animations of sea level rise (in QuickTime© format); and (4) inundation layers for use in GIS (in ESRI grid format). Each of these products is available for download from the Center for Remote Sensing of Ice Sheets (CReSIS) at http://www.cresis.ku.edu/research/data/sea_level_rise/index.html.

Acknowledgments

The authors wish to thank the following individuals for project assistance: Kalonie Hulbutta of Haskell Indian Nations University, Nathaniel Haas and Johan Feddema of the University of Kansas, and Asif Iqbal and Amber Reynolds of the Kansas Geological Survey. We also appreciate the helpful comments of the anonymous reviewers. This research was supported by the U.S. National Science Foundation under grants ANT-0424589, OPP-0122520, and HRD-0407827.

References

Dobson, J. E., E. A. Bright, P. R. Coleman, R. C. Durfee, and B. A. Worley (2000), LandScan: A global population database for estimating populations at risk, *Photogramm. Eng. Remote Sens., 66*(7), 849–857.

Dyurgerov, M. B., and M. F. Meier. (1997), Year-to-year fluctuations of global mass balance of small glaciers and their contributions to sea-level changes, *Arct. Alp. Res., 29*(4), 392–402.

Hastings, D. A., and P. K. Dunbar (1998), Development and assessment of the Global Land One-km Base Elevation Digital Elevation Model (GLOBE), *Int. Archives Photogramm. Remote Sens., 32*(4), 218–221.

Intergovernmental Panel on Climate Change (2007), *Climate Change 2007, The Physical Scientific Basis: Summary for Policymakers*, 21 pp., Geneva. (Available at http://www.ipcc.ch)

Rignot, E., and P. Kanagaratam (2006), Changes in the velocity structure of the Greenland Ice Sheet, *Science, 311*, 986–990.

NOAA National Geophysical Data Center (2001), 2-minute gridded global relief data (ETOPO2), World Data Cent. for Mar. Geol. and Geophys., Boulder, Colo. (Available at http://www.ngdc.noaa.gov/mgg/fliers/01mgg04.html)

Author Information

Rex J. Rowley, Department of Geography and Center for Remote Sensing of Ice Sheets (CReSIS), University of Kansas, Lawrence; E-mail: rjrowls@ku.edu; John C. Kostelnick, College of Mathematics and Natural Sciences, Haskell Indian Nations University, Lawrence, Kans.; David Braaten and Xingong Li, Department of Geography and CReSIS, University of Kansas, Lawrence; and Joshua Meisel, College of Mathematics and Natural Sciences, Haskell Indian Nations University, Lawrence, Kans., and CReSIS, University of Kansas, Lawrence.

How Nature Foiled the 2006 Hurricane Forecasts

PAGES 105–107

The 2006 hurricane season proved again that predicting Mother Nature is a very precarious undertaking.

At the beginning of the season, all signs indicated that it would be more active than average: Sea surface temperature (SST) was above normal, vertical wind shear was low, and sea level pressure was reduced over the tropical Atlantic. Many forecasters believed that these features foreshadowed a continuation of the trend of nine preceding years of above-normal hurricane seasons. Given the recent warming tendency in the Atlantic and the prevailing favorable preseason conditions, there was no wonder that even by August 2006, forecasters were still calling for an above-normal frequency of tropical storms and hurricanes.

By W. K. M. Lau and K.-M. Kim

In the end, however, the 2006 hurricane season was near normal with four tropical storms and five hurricanes, but decidedly lackadaisical compared with the record numbers of 12 tropical storms and 15 hurricanes in 2005. Most impressive was the fact that while five hurricanes, including Katrina, made landfall in the United States in 2005, no hurricane even came close to threatening the U.S. Gulf coast or eastern seaboard in 2006.

How did nature foil all attempts to forecast the 2006 hurricane season? Undoubtedly, this question, together with others, will be addressed by many studies to come. In this article we present new insights derived from preliminary analysis using satellite data, with the intention of stimulating further studies. Data used for this study include SST, rainfall, cloud top temperature, water vapor from the Tropical Rainfall Measuring Mission (TRMM), and aerosol index (AI) from the Ozone Monitoring Instrument (OMI) on the satellite Aura.

Tropical Storm and Hurricane Tracks

During July-August-September (JAS) 2005, there were nine distinct tropical storm and hurricane tracks over the warm pool (SST > 28°C) in the western Atlantic and Caribbean (WAC), and the Gulf of Mexico (Figure 1a). Five hurricanes made landfall over the Gulf coast and the eastern seaboard of the United States. In 2006, no hurricanes were found over the WAC and the Gulf region. Four distinct tropical storm/hurricane tracks were found at the northeastern edge of the warm pool far away from the eastern coast of the United States (Figure 1b). Only two tropical storms formed over the WAC and the eastern seaboard of the United States, but they never developed into hurricanes.

A closer look at the full hurricane season (July through November) indicates that in 2005, the tropical storm and hurricane tracks can be classified into two groups. For group 1, tropical storms were generated within 10°–15°N over the eastern Atlantic, and intensified with a clockwise track off the northwestern edge of the warm pool, east of 65°W. For group 2, tropical storms were generated and subsequently intensified to hurricane strength over the very warm water (>29°C) of the WAC